AN INVESTIGATION OF LIGHT SCATTERING BY IRREGULAR ICE

CRYSTALS VIA PSTD

A THESIS

by

JIANING ZHANG

Submitted to the Office of Graduate and Professional Studies of
Texas A&M University
in partial fulfillment of the requirements for the degree of

MASTER OF SCIENCE

Chair of Committee,	Richard Lee Panetta
Co-Chairs of Committee,	Ping Yang
Committee Members,	Sarah D. Brooks
	Benchun Duan
Head of Department,	Ping Yang

August 2014

Major Subject: Atmospheric Sciences

ABSTRACT

We implement the Pseudo-Spectral Time Domain(PSTD) algorithm with Convolutional Perfect Matched Layer(CPML). Comparisons were conducted to test its performance with Mie's method. Results illustrate its good performance. More tests are still needed to determine the validity PSTD with CPML. We propose a random field model for surface irregularities of ice crystals with roughened surfaces. Results using this model show that reflection probability decreases exponentially as the roughness is increased linearly. We also apply a holographic Muller matrix imaging technique for roughened particle characterization within this model. Simulations indicate that even a small perturbation on the surface will result in quite different patterns using this holographic Muller matrix method. This imaging method may be useful for the cloud imaging and particle characterization. We also study the effects of volume irregularities, in the form of air bubbles, on the scattering properties of ice crystals. Results show that such volume inhomogeneity leads to phase functions smoothing and the reduction of backscattering in comparison with homogeneous cases. The distribution of air bubbles in ice crystals also has a significant influence on the phase function of inhomogeneous ice crystals.

ACKNOWLEDGEMENTS

NOMENCLATURE

PSTD   Pseudo-Spectral Time Domain method

CPML   convolution perfectly matched layer

UPML   uniaxial perfectly matched layer

CFS   complex frequency shifted

IGOM   Improved geometric-optics method

DDA   Discretise dipole approximation

IHM   Inhomoge- neous Hexagonal Mono-crystal model

TABLE OF CONTENTS

LIST OF FIGURES

1. INTRODUCTION

1.1   Overview

Light scattering by atmospheric particles like ice crystals, dust, soot and aggregates. has been studied for several decades with wide applications in remote sensing, meteorology and climate research. Wave optics treatment of electromagnetic or light wave scattering involves solving the Maxwell's equations. In 1908, spherical particles scattering by electromagnetic waves was first considered by Mie in his original publication[1]. Later, Stratton[2] and Born and Wolf [3] presented comprehensive and precise foundations of Mie theory in their classic books. Extended light scattering problems and applications in atmospheric sciences or astronomy were discussed in detail in van de Hulst's book[4]. Many computational techniques have been proposed and used for solving the electromagnetic wave scattering problem, such as separation of variables method, the finite-difference time domain method, finite-element method, T-Matrix method, discrete dipole approximation and spectral method[5]. Nearly all of these methods are used in light scattering computation of atmospheric particles.

It is well accepted that cirrus clouds have a significant influence on the global climate through their radiative properties. Observations show that cirrus clouds are composed of ice crystals with various shapes and sizes. The scattering properties of these particles have been widely studied[6, 7, 8, 9, 10]. For example, a geometrical optics based method on ray-tracing and Monte-Carlo techniques was used for inhomogeneous ice crystals[12]. Results have shown that phase functions of inhomogeneous ice crystals with bubbles are smoothed, the 22° and 46° halo peaks are swept out, backscattering is reduced[13]. In this thesis, we use the much more accu-

rate PSTD method to study the effect of inhomogeneity. We also use the method to study the effects of surface roughness. Studies have shown that the surface roughness play an important role in determining the single-scattering properties of the particles. In particular, the study by Zhou et al[14], of horizontally oriented crystals using CALIPSO's observations was a motivation for our work.

In this thesis, we simulated the light scattering by horizontally oriented ice crystals with surface irregularity and volume irregularity via the PSTD method[18]. As is well known, the spectral method is a very powerful approach for solving partial differential equations(PDEs)[15]. The fundamental idea behind spectral methods is to approximate solutions of PDEs by finite series of orthogonal basis functions such as the complex exponentials or Chebyshev polynomials. In our approach, we apply Roden's convolutional-PML(CPML) method to the collocated PSTD method for the boundaries[16]. The CPML shows performance improvement over previous artificial absorbing boundaries.

1.2 Electromagnetic Scattering Theory

In this section, we introduce some basic theory and definitions, which we will use frequently afterward. The Maxwell equations are the set of four fundamental equations governing electromagnetic fields. Maxwell's equations for a traveling wave in a source free linear medium with a relative permittivity ε, relative permeability μ in natural units are

$$\nabla \times \mathscr{H} = \varepsilon \frac{\partial \mathscr{E}}{\partial t}, \tag{1.1}$$

$$\nabla \times \mathscr{E} = -\mu \frac{\partial \mathscr{H}}{\partial t}, \tag{1.2}$$

$$\nabla \cdot \mathscr{H} = 0, \tag{1.3}$$

$$\nabla \cdot \mathscr{E} = 0. \tag{1.4}$$

$\mathscr{E}$ and $\mathscr{H}$ represent the electric field and magnetic field respectively. The introduction of a particle in the medium results in scattering. For a plane wave illumination, the total field thenconsists of a incident plane field and a scattered spherical field. At a large distance from the scatterer, we have the total field in the asymptotic form:

$$\mathscr{E} \simeq \mathscr{E}_{inc} e^{i\mathbf{k}\cdot\mathbf{r}} + \mathscr{E}_{scatt} \frac{e^{ikr}}{r}, \tag{1.5}$$

$$\tag{1.6}$$

where $\mathbf{k} = k\hat{\mathbf{r}}$, is the wave number, $\mathscr{E}_{inc}, \mathscr{E}_{scatt}$ are the complex amplitudes of incident and scattered electric fields. Then, let us consider electric field decomposed mutually perpendicular components, parallel($\mathscr{E}_{\parallel}$) and perpendicular($\mathscr{E}_{\perp}$) to the reference plane:

$$\mathscr{E} = \mathscr{E}_{\parallel} \hat{\mathbf{e}}_{\parallel} + \mathscr{E}_{\perp} \hat{\mathbf{e}}_{\perp} \tag{1.7}$$

Where $\hat{\mathbf{e}}_{\parallel}, \hat{\mathbf{e}}_{\perp}$ are unit vectors in directions parallel and perpendicular to the plane. Due to the linearity of Maxwell's equations, the scattered field is proportional to the incident field.

$$\begin{pmatrix} \mathscr{E}_{\parallel} \\ \mathscr{E}_{\perp} \end{pmatrix}_{scatt} = \begin{pmatrix} S_1 & S_2 \\ S_3 & S_4 \end{pmatrix} \begin{pmatrix} \mathscr{E}_{\parallel} \\ \mathscr{E}_{\perp} \end{pmatrix}_{inc}$$

Here $S_i, i = (1, 2, 3, 4)$ are components of the amplitude scattering matrix. The Stokes vector $|\mathscr{S}\rangle$ (with I, Q, U, V its parameters) is defined as:

$$|\mathscr{S}\rangle = \begin{pmatrix} I \\ Q \\ U \\ V \end{pmatrix} = \begin{pmatrix} |\mathscr{E}_\parallel|^2 + |\mathscr{E}_\perp|^2 \\ |\mathscr{E}_\parallel|^2 - |\mathscr{E}_\perp|^2 \\ -2\mathrm{Re}(\mathscr{E}_\parallel \mathscr{E}_\perp^*) \\ -2\mathrm{Im}(\mathscr{E}_\parallel \mathscr{E}_\perp^*) \end{pmatrix} \tag{1.8}$$

Here $\mathscr{E}_\eta^*, (\eta = \parallel, \perp)$ denotes the conjugate of $\mathscr{E}_\eta$. We emphasize that the representation of Stokes vectors depends on the choice of the plane of reference (see Fig 1.1), a different reference of plane leads to a difference coefficients.
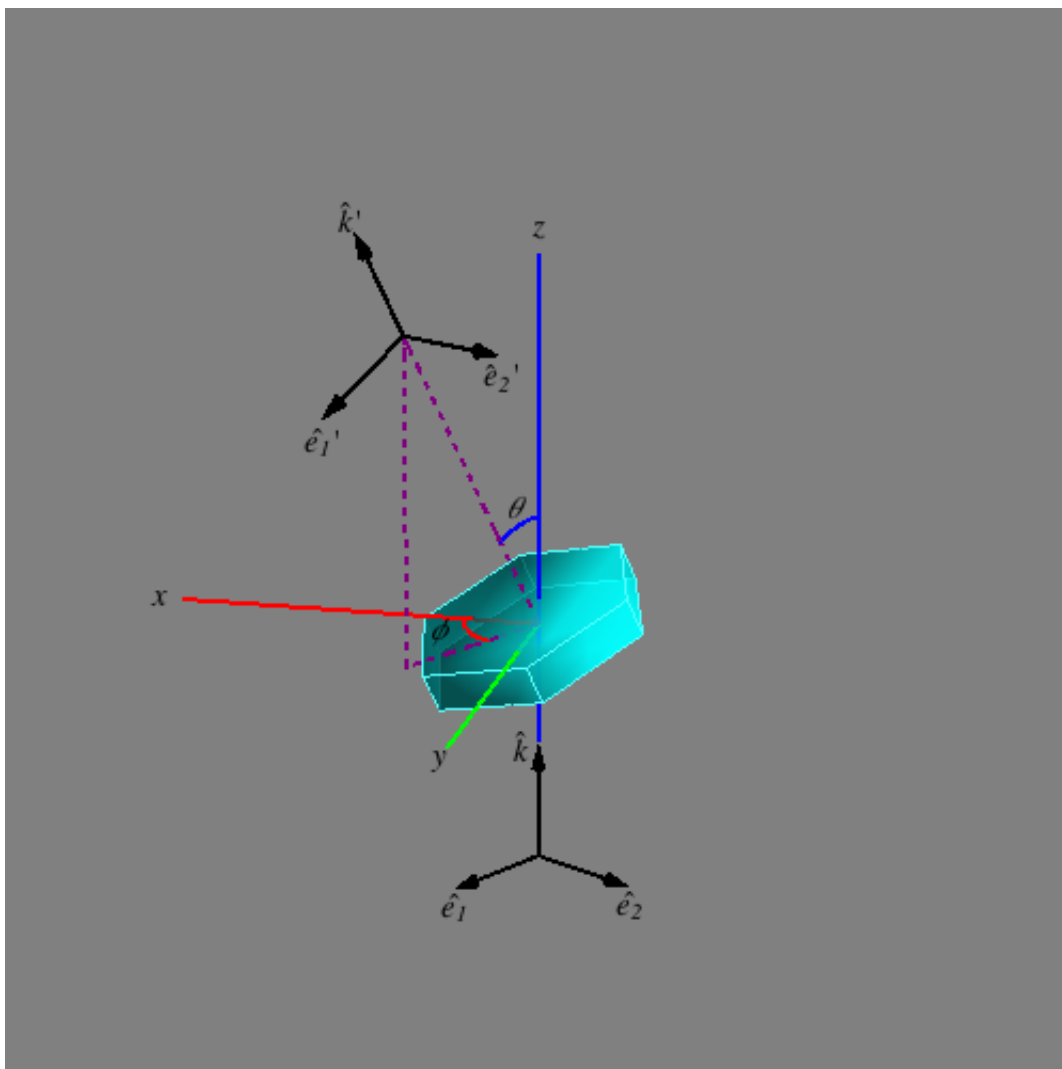
Figure 1.1: Scattering Geometry

The relation between these components of the Stokes vector for a completely coherent wave is

$$I^2 = Q^2 + U^2 + V^2$$

In general, we have $I^2 \geq Q^2 + U^2 + V^2$. The Stokes vectors of incident and scattered fields are linked by the Mueller matrix $\hat{M}$ or by the related phase matrix $\hat{P}$:

$$|\mathscr{S}\rangle_{scatt} = \hat{M}|\mathscr{S}\rangle_{inc} = \frac{\sigma_s}{4\pi}\hat{P}|\mathscr{S}\rangle_{inc}$$

Where σ_s is the scattering cross-section. We canthus write it expectedly

$$\begin{pmatrix} I \\ Q \\ U \\ V \end{pmatrix}_{scatt} = \frac{\sigma_s}{4\pi} \begin{pmatrix} P_{11} & P_{12} & P_{13} & P_{14} \\ P_{21} & P_{22} & P_{23} & P_{24} \\ P_{31} & P_{32} & P_{33} & P_{34} \\ P_{41} & P_{42} & P_{43} & P_{44} \end{pmatrix} \begin{pmatrix} I \\ Q \\ U \\ V \end{pmatrix}_{inc}$$

We note that

$$\frac{\sigma_s}{4\pi}P_{11}(\theta, \phi) = \frac{I_{scatt}}{I_{inc}} = \frac{d}{d\Omega}\sigma_s$$

and

$$\int P_{11}(\theta, \phi)\frac{d\Omega}{4\pi} = 1$$

P_{11} is called the phase function is the probability for scattering of unpolarized incident light in any direction θ, ϕ.

2. SPECTRAL METHOD AND PERFECTLY MATCHED LAYER

2.1 Spectral Method

How we approximate and represent spatial differential operators leads to such different approaches for solving PDEs, las the Finite-Difference, Finite Element and Spectral methods. Formally, we write

$$\partial_x \psi(x) \approx \mathscr{D}_x \psi(x), \tag{2.1}$$

$\mathscr{D}_x$ is the approximate differential operator. As a very powerful approach for solving PDEs[15], the fundamental idea behind spectral methods is to approximate solutions of PDEs by finite series of orthogonal basis functions, and there are essentially three steps that we have to make to derive a spectral method: what the basis functions should be used, how the approximation will be written, and which procedure the solution is determined in.

In spectral methods, square integrable functions are typically expanded as sum of orthogonal basis functions. The solution functions are expanded as a finite series of continuous orthogonal basis functions, which is called model expansion. However, in most cases, it is not easy to analytically evaluate the integrals involved in the expansion coefficients. An alternative is to approximate the integrals by interplants of grid points("node"). This interpolation formulation is similar to that taken in finite difference method where the unknowns are the values at grid points in spatial coordinates. In finite difference method, derivatives of solution functions are approximated grid points by the derivative of a polynomial that interpolates the function through the point and close neighbors. Such an approximation is usually called a

nodal approximation. The methods using nodal approximation to representat the functions are called Pseudo-Spectral methods and have been frequently used for solving partial differential equations. A principle advantage of the PS methods is that its comp can be considerably accelerated by the use of fast Fourier transform(FFT).

The Fourier Pseudo-Spectral method applies fast Fourier transforms $\mathscr{F}$ to approximate the differential operator $\mathscr{D}_x$ as follows:

$$\mathscr{D}_x \psi(x) = \mathscr{F}_x^{-1}[ik_x \mathscr{F}_x]\psi(x), \qquad (2.2)$$

The $\mathscr{F}$ is the FFT operator, $\mathscr{F}^{-1}$ is its inverse FFT operator.

2.2 PSTD

The finite-difference time-domain (FDTD) method has been considered as a simple, robust and powerful technique of the full-wave techniques used to light scattering problem[16]. It can accurately tackle a wide range of problems. However, as with all numerical methods, it has been founded that FDTD is only applicable for rather small particles even with parallel computing techniques, the computational time increases too rapidly with increasing particle size [17]. In order to solve scattering problems for large particles, researchers have proposed various techniques to improve the method[5]. One of them is the pseudospectral time-domain method which uses spectral methods to approximate spatial derivatives of Maxwell's equations[18]. The PSTD method has been developed for both unbounded and bounded media, and has been shown to outperform the FDTD methods, especially for large particle scattering problems.

After discretization of Maxwell's equations, the governing equations are

$$E_x|_{i,j,k}^{n+1/2} = E_x|_{i,j,k}^{n-1/2} + \frac{\delta t}{\epsilon_r|_{i,j,k}}\{\mathscr{F}_y^{-1}[jk_y\mathscr{F}_y(H_z)]|_{i,j,k}^n - \mathscr{F}_z^{-1}[jk_z\mathscr{F}_z(H_y)]|_{i,j,k}^n\} \quad (2.3)$$

$$E_y|_{i,j,k}^{n+1/2} = E_y|_{i,j,k}^{n-1/2} + \frac{\delta t}{\epsilon_r|_{i,j,k}}\{\mathscr{F}_z^{-1}[jk_z\mathscr{F}_z(H_x)]|_{i,j,k}^n - \mathscr{F}_x^{-1}[jk_x\mathscr{F}_x(H_z)]|_{i,j,k}^n\} \quad (2.4)$$

$$E_z|_{i,j,k}^{n+1/2} = E_z|_{i,j,k}^{n-1/2} + \frac{\delta t}{\epsilon_r|_{i,j,k}}\{\mathscr{F}_x^{-1}[jk_x\mathscr{F}_x(H_y)]|_{i,j,k}^n - \mathscr{F}_y^{-1}[jk_y\mathscr{F}_y(H_x)]|_{i,j,k}^n\} \quad (2.5)$$

$$H_x|_{i,j,k}^{n+1} = H_x|_{i,j,k}^n - \frac{\delta t}{\mu_r|_{i,j,k}}\{\mathscr{F}_y^{-1}[jk_y\mathscr{F}_y(E_z)]|_{i,j,k}^n - \mathscr{F}_z^{-1}[jk_z\mathscr{F}_z(E_y)]|_{i,j,k}^{n+1/2}\} \quad (2.6)$$

$$H_y|_{i,j,k}^{n+1} = H_y|_{i,j,k}^n - \frac{\delta t}{\mu_r|_{i,j,k}}\{\mathscr{F}_z^{-1}[jk_z\mathscr{F}_z(E_x)]|_{i,j,k}^n - \mathscr{F}_x^{-1}[jk_x\mathscr{F}_x(E_z)]|_{i,j,k}^{n+1/2}\} \quad (2.7)$$

$$H_z|_{i,j,k}^{n+1} = H_z|_{i,j,k}^n - \frac{\delta t}{\mu_r|_{i,j,k}}\{\mathscr{F}_x^{-1}[jk_x\mathscr{F}_x(E_y)]|_{i,j,k}^n - \mathscr{F}_y^{-1}[jk_y\mathscr{F}_y(E_x)]|_{i,j,k}^{n+1/2}\} \quad (2.8)$$

i, j, k are indexes of spatial coordinates, n is time index and δt is the time step. The total EM field components can be decomposed into incident and scattered terms $E_{total} = E_{inc} + E_{scatt}$. Our purpose is to compute the properties of the scattered field. To obtain governing equations for the E_{scatt}, a source term [19] for incident fields must be added to the right of these electromagnetic fields equations:

$$(1 - \varepsilon_r|_{i,j,k})(\frac{\partial E_{\eta,inc}}{\partial t})|_{i,j,k}^n \quad (\eta = x, y, z)$$

$E_{\eta,inc}$ is the incident field, $\varepsilon_r|_{i,j,k}$ is the dielectric constant at specific grid point.

2.3 Perfectly Matched Layer

In the mid 1990s, Jeanne-Pierre Berenger first proposed the idea of a perfectly matched layer(PML), an artificial absorbing boundary regions to make possible a finite computational domain in wave propagation simulations[20][21]. The PML is designed to have the characteristics that electromagnetic waves of arbitrarily po-

9

larization and any frequency impinging on a PML region will be absorbed in the medium without reflection. Several formulations of PML have been proposed. A split-field formulation of Maxwell's equations was used in Berenger's original PML. After that, it was illustrated by Chew et al. that Berenger's PML was equivalent to expressing Maxwell's equation in complex-stretched coordinates[22]. Sacks et al. later proposed the uniaxial perfectly matched layer(UPML), in which the PML was considered as an artificial anisotropic medium.

In this thesis, we apply instead Roden's convolutional-PML(CPML) method to the collocated PSTD method with Complex-Frequency-Shifted(CFS) PML constitutive parameters. Although CPML is believed to be the most robust and computationally efficient method for use with a FDTD calculation using Yee's algorithm, it is not quite sure how about the performance with a collocated grid has not been studied. Before we discuss its performance, we give a brief review of CPML. First, we write the Ampere's law in the frequency domain for the x component of electric field.

$$j\omega E_x + \sigma_x E_x = \frac{1}{s_y}\frac{\partial}{\partial y}H_z - \frac{1}{s_z}\frac{\partial}{\partial z}H_y \tag{2.9}$$

ω is the frequency. σ_η is conductivity for absorbing the incident wave to the PML region. Complex-Frequency Shifted (CFS)[16] stretched parameters$s_\eta, \eta = x, y, z$ in the stretched coordinate formulation[22] are expressed as

$$s_\eta = \kappa_\eta + \frac{\sigma_\eta}{a_x + j\omega} \tag{2.10}$$

$j = \sqrt{-1}$, a_x and κ_x are constitutive parameters. These parameters are spatially scaled to eliminate the reflection waves. Then, we transform the Maxwell's

equations to time domain and discretized them. The stretched parameters s_η becomes functions of time. The spatial derivative terms become the convolution of time domain stretched parametersand EM fields derivatives. We can then apply a recursive method to solve this convolution. In the following we will review how these parameters are scaled and the recursive convolution method are applied.

We define the PML constitutive parameters as the one-dimensional functions: $s_x(x), s_y(y)$, and $s_z(z)$, where σ_x and κ_x are also one-dimensional functions of x. An appropriate scaling function is a polynomial scaling[16] such that:

$$\sigma_x(x) = \begin{cases} \frac{|x-x_o|^m}{d^m}\sigma_x^{max}, & x_o \leq x \leq x_o + d, \\ 0, & \text{otherwise.} \end{cases} \tag{2.11}$$

$$\kappa_x(x) = \begin{cases} 1 + \frac{|x-x_o|^m}{d^m}(\kappa_x^{max} - 1), & x_o \leq x \leq x_o + d, \\ 1, & \text{otherwise.} \end{cases} \tag{2.12}$$

Here x_o is the x-coordinate of the PML interface, d is the thickness of the PML layer, and σ_x^{max} is the maximum value of σ_x at $x = x_o + d$. Similarly, κ_x^{max} is the maximum value of κ_x at $x = x_o + d$. It has also been found[16] that the optimal value of m typically is in the range of $3 \leq m \leq 4$.

It is necessary to point that $a_x$must be much larger than σ_x to eliminate low frequency reflection errors at the front boundary interface and small enough within the PML in order to improve the attenuation of low-frequency waves. Hence, it follows that a_x should be scaled as a function of x in a manner such that it is maximum at x_o, and minimum at the ending boundary $x_o + d$. This is opposite of how σ_x and κ_x were scaled.

$$a_x(x) = \begin{cases} |\frac{d+x-x_o}{d}|^m a_x^{max}, & x_o \le x \le x_o + d, \\ 0, & \text{else.} \end{cases} \tag{2.13}$$

Finally, consider the x-projection of the magnetic field as expressed in PML region with CFS-PML tensor parameters[24] defined above:

$$-\mu \frac{\partial}{\partial t} H_x = \frac{1}{\kappa_y} \frac{\partial}{\partial y} E_z - \frac{1}{\kappa_z} \frac{\partial}{\partial z} E_y + q_{y,z}^E - q_{z,y}^E \tag{2.14}$$

with the auxiliary variables $q_{y,z}^E$ obeying the Auxiliary Differential Equation (ADE)[24]:

$$q_{y,z}^E = b_y q_{y,z}^E - c_y \frac{\partial}{\partial y} E_z \tag{2.15}$$

Other auxiliary variables $q_{x,y}^E, q_{x,z}^E, q_{y,x}^E, q_{z,x}^E, q_{z,y}^E, q_{x,y}^H, q_{x,z}^H, q_{y,x}^H, q_{z,x}^E and q_{z,y}^E$ follow similar equations, which we omit. For the parameters in the ADE, we have[16]

$$b_y = e^{-\Delta t/\tau}, \quad c_y = \frac{\sigma_y}{\kappa_y} \frac{1}{(\kappa_y a_y + \sigma_y)} (1 - e^{-\Delta t/\tau})$$
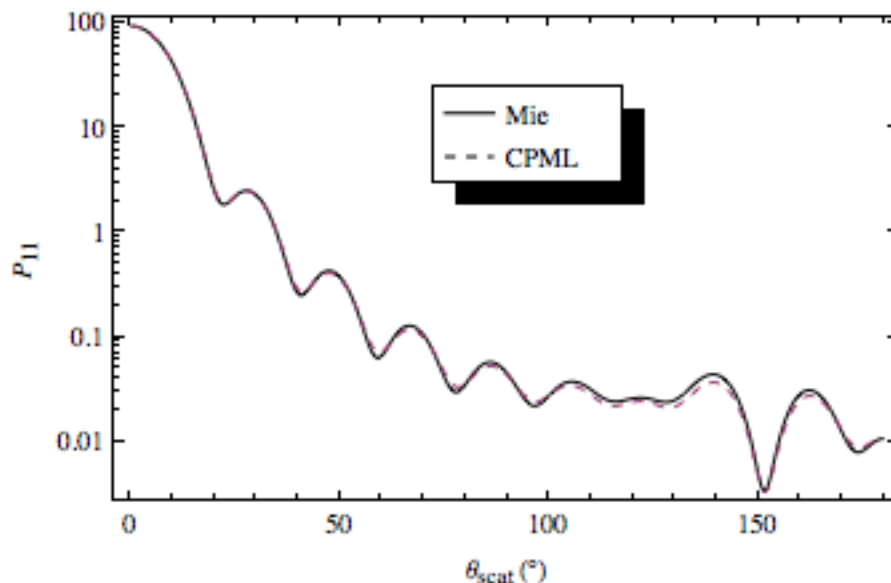
Figure 2.1: Comparition between phase functions of dielectric Sphere with refractive index 1.2 and size parameter 10 computed from Mie's method and CPML-PSTD algorithm

To test the PSTD with CPML, the problem of light wave scattering by a dielectric sphere is studied. Specifically, a sphere of size parameter 10 and refractive index 1.2 is placed in vacuum. A modulated Gaussian wave packet with central frequency 0.000001 is injected into computation domain. The resolution is set to be 15. 6 cell thick PML layers terminate, 5 layers from the scatter region, $72 \times 72 \times 72$ lattice in total. Within the PML region, σ_η, κ_η and α_η^{max} are scaled using an $m = 4$ polynomial scaling, with $\sigma_\eta^{max} = \frac{0.8(m+1)}{\Delta}$ and $\kappa_\eta^{max} = 1.1$, and $\alpha_\eta^{max} = 0.1$ respectively. The Fig 2.1 compare phase functions of dielectric Sphere with refractive index 1.2 and size parameter 10 computed from Mie's method and CPML-PSTD algorithm. It shows quite well agreement for them, especially for the backscattering direction. Although more tests are still need for certification of the validity. The Fig. 2.2 illustrates a snapshot of the wave propagating through the particle.

To investigate the reflection error due from CPML, a 2D PSTDsimulation with 60 cells in each dimension was conducted with the same CPML parameters. However, in this simulation, a total field formulation with sinusoidal wave sources was used in our case. The error relative to a reference field(exact field without refection error) was computed as a function of simulation steps[24]:

$$\text{error} = 20\text{Log}(\frac{|\psi(\text{t}) - \psi_{\text{ref}}(\text{t})|}{|\psi_{\text{ref}}^{\text{max}}|})$$

where $\psi(t), \psi_{\text{ref}}(t)$ represent the simulated field and reference field respectively.
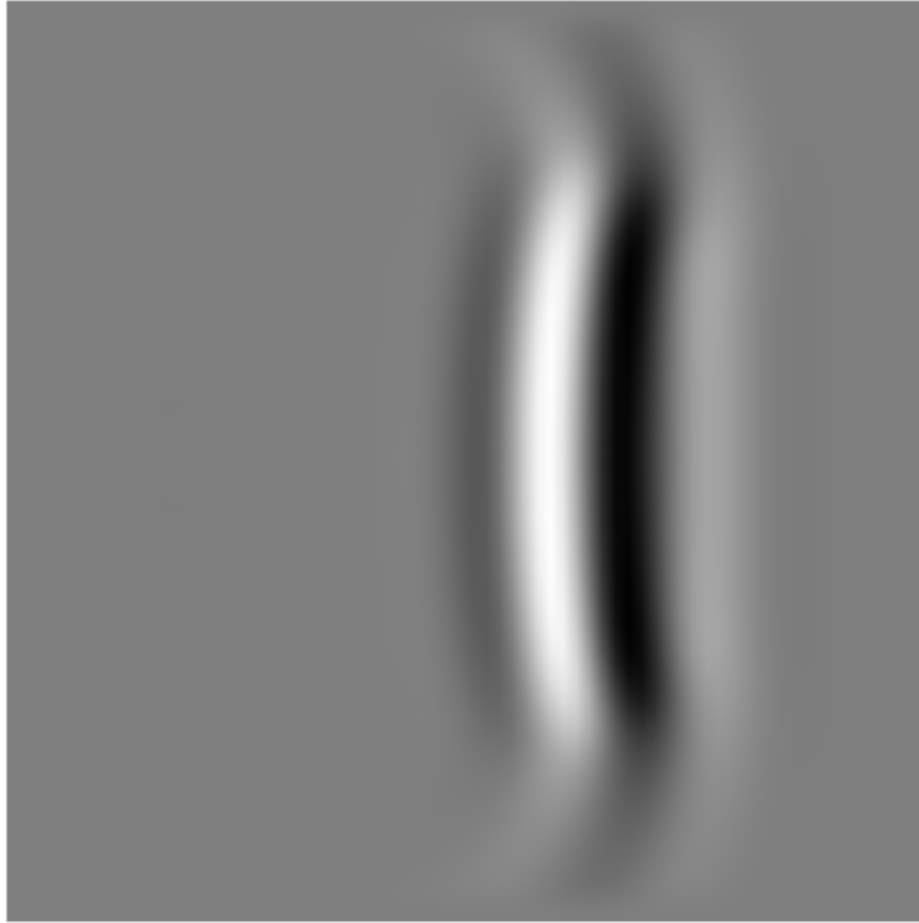
Figure 2.2: Snapshot of the scattered electric field E_x scattered by a dielectric sphere with size parameter 10 and refractive index 1.2.

But studies have show that these two PML schemes have similar absorbing ability[25].

3. SCATTERING PROPERTIES OF IRREGULAR ATMOSPHERIC ICE CRYSTALS

3.1 Motivation

Cirrus clouds play an essential role in modulating climate and atmospheric radiation transfer. It is widely known from simulations that the shapes and sizes of ice crystals are quite important in the single-scattering by atmospheric ice crystals[9, 10, 26, 27]. Compared with surface roughness affects on light scattering, the effects of shaw and size have been more widely studied. However, no perfect ice crystal will exist in nature: every real ice crystal will suffer from defects, deformation, inhomogeneity and roughness of some kind[28, 29, 30, 31]. It is crucial to understand to what extent these imperfections will influence the scattering and radiation properties of ice crystals. In previous work, both geometric optics and wave optics methods have been used to address such issues[9, 10]. For example, single scattering ray-tracing studies have been used in roughened hexagonal ice crystals by random-tilt algorithms, in which light rays propagating through the interface are randomly redirected. These studies indicate that surface roughness and inhomogeneity will influence scattering properties significantly. The ice crystals are usually considered to be randomly oriented in these studies.[14, 33]. Here, we investigate how surface roughness influences the radiation properties of horizontally oriented plates, especially the phase function. We predict that such case may have measurable effects in remote sensing and climate research. On the other hand, aircraft-deployed cloud imaging instruments provide a way for characterizing shapes and even surface characteristic of ice crystals[34]. However, all these imaging schemes involve intensity measurement. Here, we also show a Muller matrix holographic imaging technique involving measuring the polarization

properties of light, that has potential for application in cloud particle imaging[35].

3.2 Scattering By Surface Irregular Particles

3.2.1 Modeling of Rough Surfaces

All real surfaces, even those carefully fabricated ones, are rough to some degree. However, the dynamics of ice crystals' surfaces involve a lot of complicated physical processes: deposition, evaporation, collision and so on. Recently, Pfalzgraff et al.[36]. present photos on ice crystal surfaces of growing and ablating via scanning electron microscopy. Although these ice crystals were formed in the lab, their relevance to cirrus particles has been argued. On the scale more than $10\mu m$, modeling of microphysics on cirrus cloud crystal has attained a considerable success[36]. Various crystals habits have been observed and studied like bullets, hollows, aggregates and so on. Laboratory researches have shown the dependency of crystal habit on temperature, supersaturation and other factors[36]. However, little information is available concerning cirrus ice crystals, the surface dynamics of t especially what defermined the roughness scale. Yet it is believed that the scale of roughness heavily influence the scattering and radiation properties. Molecular dynamical simulation has provide some insight into the physical and chemical processes. But the exact mechanism is still far from being understood.

In our simulations, we use random field models to describe the morphology of the ice crystal surface. When the surface height function is independent of direction, the surface is called isotropic, otherwise it is called anisotropic. Recent work has shown the existence of anisotropic surface features on ice crystals[36]. The statistics of geometrical features of random fields such as the density of extrema of various types, can be used to characterize the fields. In the case that the fields can be approximated as Gaussian fields, the physical meaning of these fields is generally

well understood. Although analytical investigations are often limited to Gaussian fields, phenomena described by nonlinear laws typically produce non-Gaussian signals. Even tiny departures from Gaussianity may indicate in a crucial signature of the nonlinear mechanisms at the heart of the surface dynamics. But whether a non-Gaussian model will bring any difference in light scattering is still unknown.

The next question is how to generate random fields numerically with different parameters for our light scattering model. We use a convolution method to generate the random field[37]. In the literature, Yang and Liou used a Gaussian model to generate the surface for ray tracing techniques[10]. We point out that what the difference between these models is a correlation function they use. All of them are gaussian models and can be generated in our more general random fields model. To gain more insights into the physical mechanisms that govern our random surfaces(see Fig. 3.1), let us consider first how an isotropic Gaussian field h arises from the random superposition of waves[40]:

$$h(\vec{r}) = \sum_{\vec{k}} A(k) cos(\vec{k} \cdot \vec{r} + \phi_{\vec{k}}) \tag{3.1}$$

$A(k)$ is the an amplitude spectrum that depends only on the magnitude of the wave vectors $\vec{k}$. The uncorrelated random phases $\phi_{\vec{k}}$ are uniformly distributed in the range $[0, 2\pi]$. The power spectrum is $P(k) = A(k)^2$, containing the two-point correlation of random fields. The statistical properties of the $h(\vec{r})$ are entirely encoded by the power function $P(k)$ and the moments generated from it.

(a) $P(k) = 1/k^2$

(b) $P(k) = 1/k^4$

(c) $P(k) = 1$
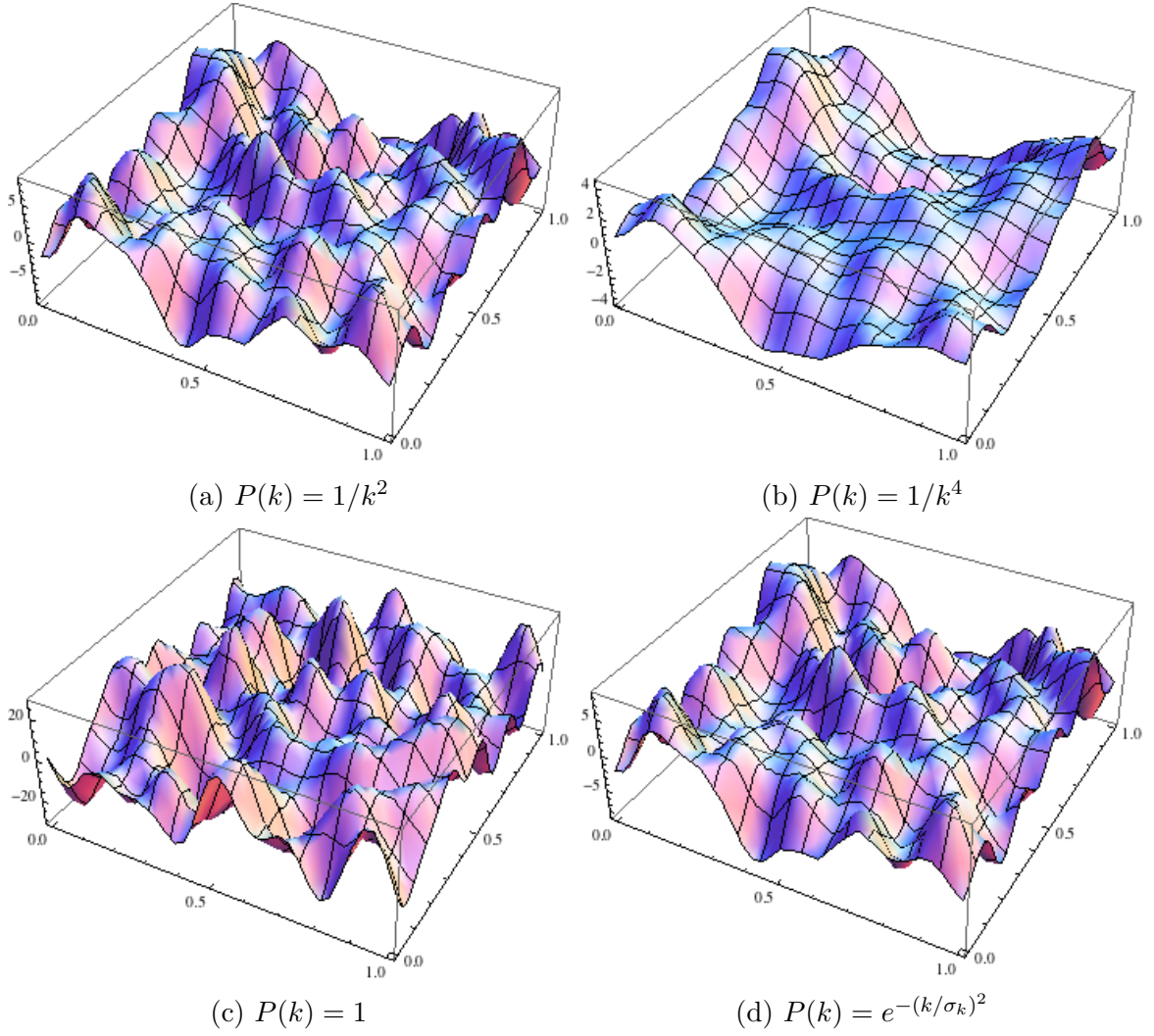
(d) $P(k) = e^{-(k/\sigma_k)^2}$

Figure 3.1: Gaussian random surface generated from different power functions.(a) $P(k) = 1/k^2$ (b) $P(k) = 1/k^4$ (c) Write noise: $P(k) = 1$ (d)Gaussian type power function: $P(k) = e^{-(k/\sigma_k)^2}$

In our model, two kinds of roughening were used: one with anisotropic roughening in the prismatic plane; the other is isotropic roughening on the top and bottom surface. The size parameter of the particle is 100 and the wave length is 0.65 μm. For the roughness, we have generate an isotropic Gaussian random field on top/bottom surfaces of the crystal and the side surface, we have use a more anisotropic fields [29].

19

The scale are measured in the length of wave length. We apply the PSTD method to compute the scattering properties of roughened particles with size parameter 150. Incident waves were traveling through the particle from the top to the bottom of the plates. The refractive index of ice crystals was $1.308 + i1.4300e - 8$. For a smooth ice crystal, the spherical distribution of P_{11} indicates symmetric features. We could see the evidence of side faces clearly. The features of P_{11} were smoothed as the height of the surface increased. As a smooth particle was roughened, more back scattering reflectance was observed. We have defined a rough degree for the surface :

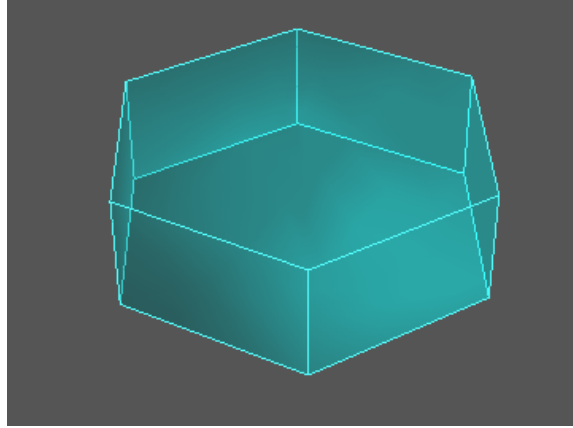$$\Delta_r = \max(h(\tilde{x}, t))/\lambda \tag{3.2}$$

Figure 3.2: Hexagonal ice plate

Backscattering enhancement from metal rough surfaces has been proposed in theory and observed both experimentally and numerically[39]. There are two mechanism contributing for the enhancement: one is for the large height and slope, the other is the surface wave's existence. While our results showed that backscattering radiation

20

was highly reduced with the increase of the mean surface height for ice crystal plates in Fig 3.2. We define a quantity called reflection ratio:

$$\text{reflection} \quad \text{ratio} = \frac{P_{11}(\theta = 180°, \Delta_r)}{P_{11}(\theta = 180°, \Delta_r = 0)} \tag{3.3}$$
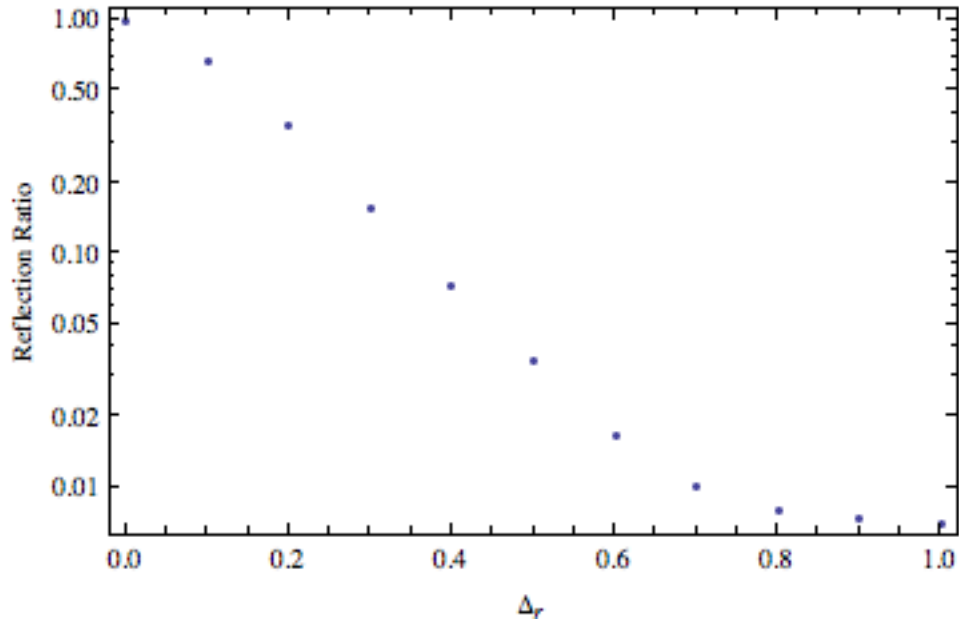

Figure 3.3: Reflection ratio as a function of roughness degree

As illustrated in Fig 3.3 , the probability of backscattering decay exponentially as we linearly increase the height of roughness. Results show that reflection ratio decrease exponentially as we increase the rough degree linearly. While the backscattering decrease much more slowly if the incident wave are from $30°$(Fig 3.4).
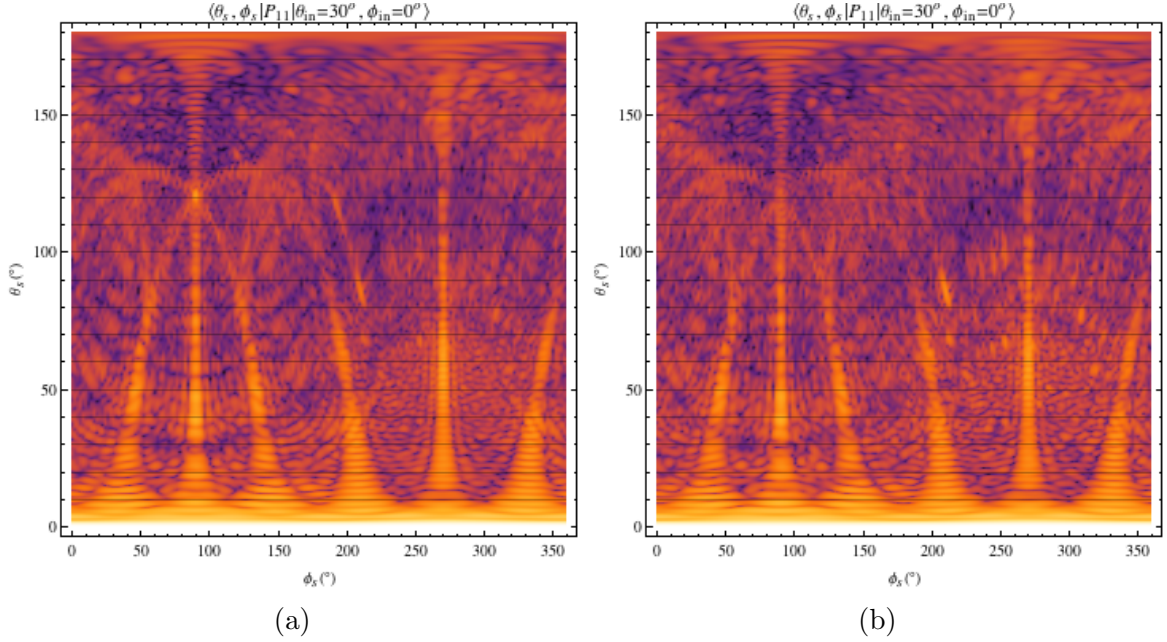
Figure 3.4: Phase function of rough ice plate illuminated from $\theta_{inc} = 30°$ with size parameter 150 for different rough degrees (a) $\Delta_r = 0.25$ (b) $\Delta_r = 0.5$

In Zhou's research[14], if 2% of total particles are smooth, simulations will provide a well agreement with real observations. Our findings show that much more horizontally oriented particles is needed to get similar features. The peaks of scattering were swept out gradually. The texture of the phase matrix over solid angles attend to be more subtle. Compared with prismatic plane roughness, the roughness of top/bottom surfaces plays a much more important role in scattering. We have set the wave incident into the particle from the top. The the wave length λ is important quantity for roughness effects observation. We note that since the roughness of naturally occurring ice crystals is related to the temperature of their environment, knowledge of effects of roughness on scattering may lead to a way of estimating cloud temperature.

3.2.2 Mueller Matrix Holographic Imaging For Roughened Ice Crystal

Holography has been extensively studied for the past 50 years[34]. With the development of electronic imaging devices like CCD, it is now possible to capture the interference pattern in real time. This holographic pattern imaging technique is often referred as the holographic imaging. Recently, a new holographic method based on Mueller holographic matrix has been developed[35]. The incident field is transformed into the interference light field described by a 4 by 4 holographic Mueller matrix, which contains all the polarization information. It is believed that such a method could be used for atmospheric particle characterization. We will give a brief description of this method: see[35].

$$\hat{M}' = \hat{1} + \frac{1}{k^2 r^2} \hat{M} + \hat{M}^h \tag{3.4}$$

$$|\mathscr{S}\rangle_{scatt} = \hat{M}|\mathscr{S}\rangle_{inc}$$

For details, the total field Mueller matrix $\hat{M}'$ is decomposed into three parts, where $\hat{M}$ relates the incident and scattered stokes vectors. $\hat{1}$ is the incident field matrix, and $\hat{M}^h$ is the holographic Mueller matrix. $|\mathscr{S}\rangle_{inc}$ and $|\mathscr{S}\rangle_{scatt}$ are incident and scattering Stokes vectors. In the far field zone, the second term on the right hand side of (3.4) can be neglected.
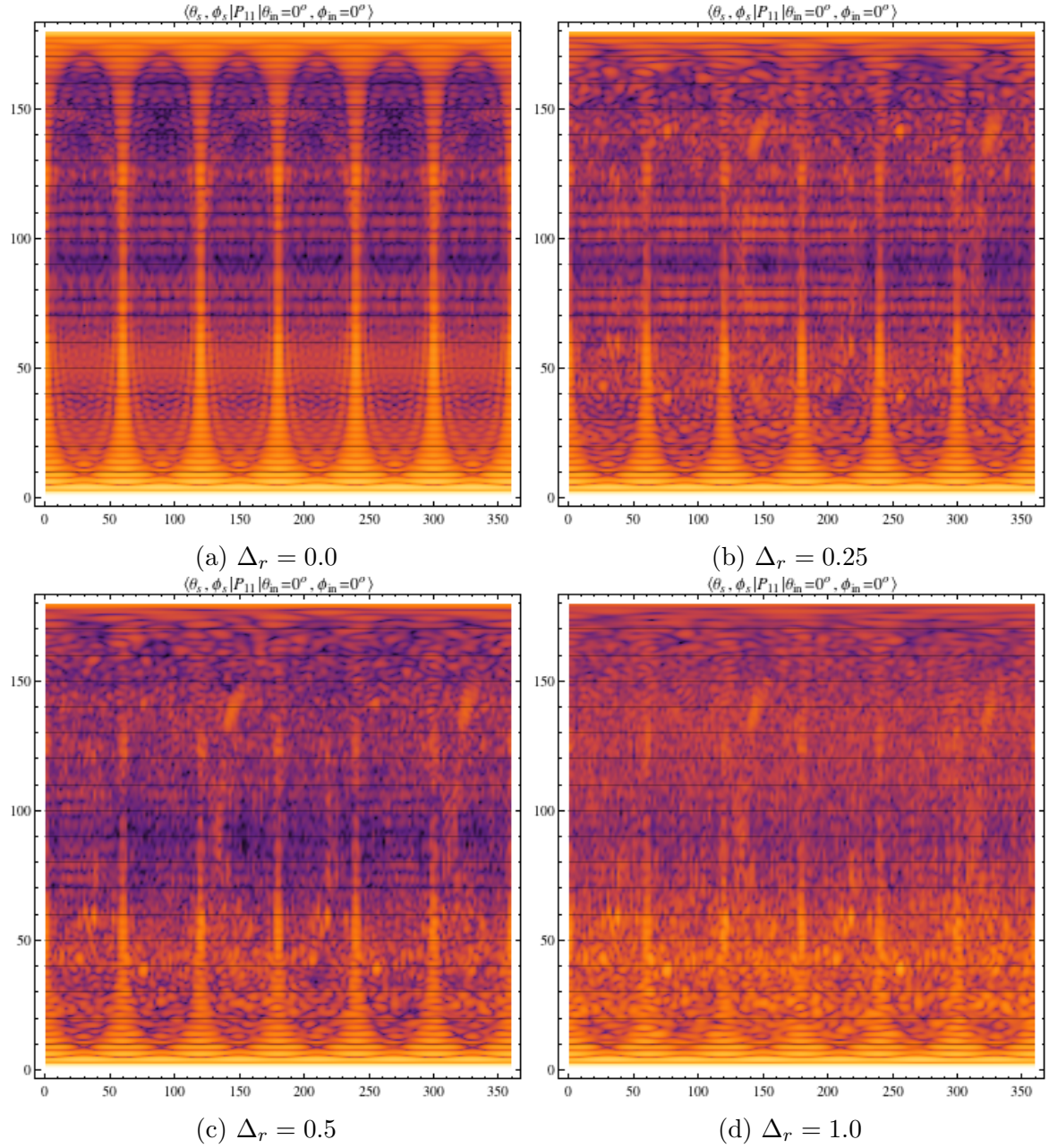
Figure 3.5: Phase function of rough ice plate illuminated from $\theta_{inc} = 0°$ with size parameter 150 for different rough degrees (a) $\Delta_r = 0.0$ (b) $\Delta_r = 0.25$ (c) $\Delta_r = 0.5$ (d) $\Delta_r = 1.0$

In our numerical studies, we chose the same ice crystals with rough surfaces as

before. The patterns of the holographic Mueller matrix for hexagonal ice crystals were computed by the PSTD method. The imaging plane was placed 50λ ahead of the particle. Again, we increased the roughneww degree from zero to the scale of incident wavelength "λ". The holographic Mueller matrix Fig. 3.5shows a quite sensitive signature of the roughness. As the roughness increases, the symmetry in the images breaks gradually. Potential application may exist for using features of the holographic Mueller matrix (Fig. 3.6 Fig. 3.7 Fig. 3.8 Fig. 3.9) to characterize the roughness of ice crystals.

Figure 3.6: Angular distribution of M_{11}^h size parameter and Δ_r varies as in Fig 3.5

(a) $\Delta_r = 0.0$

(b) $\Delta_r = 0.25$

(c) $\Delta_r = 0.5$
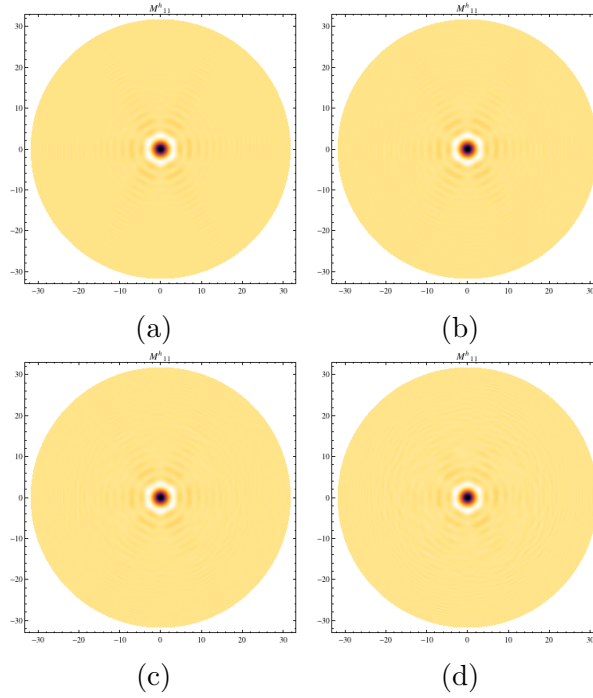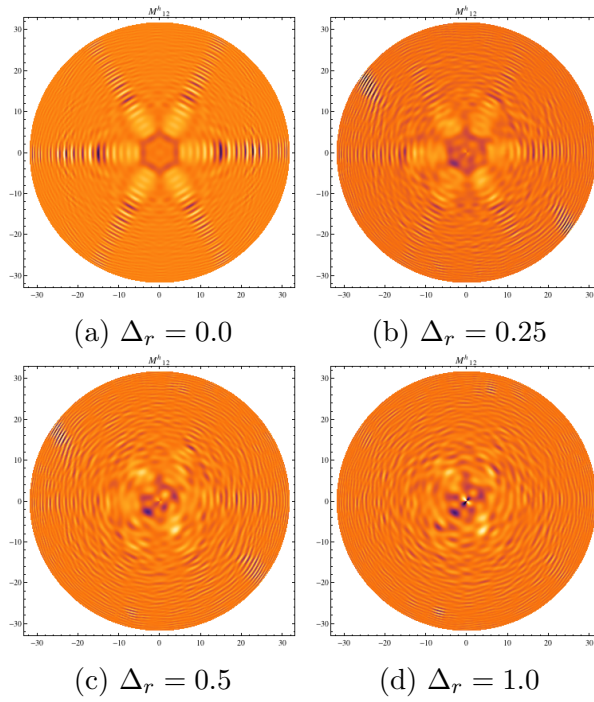
(d) $\Delta_r = 1.0$

Figure 3.7: Angular distribution of M_{12}^h size parameter and Δ_r varies as in Fig 3.5
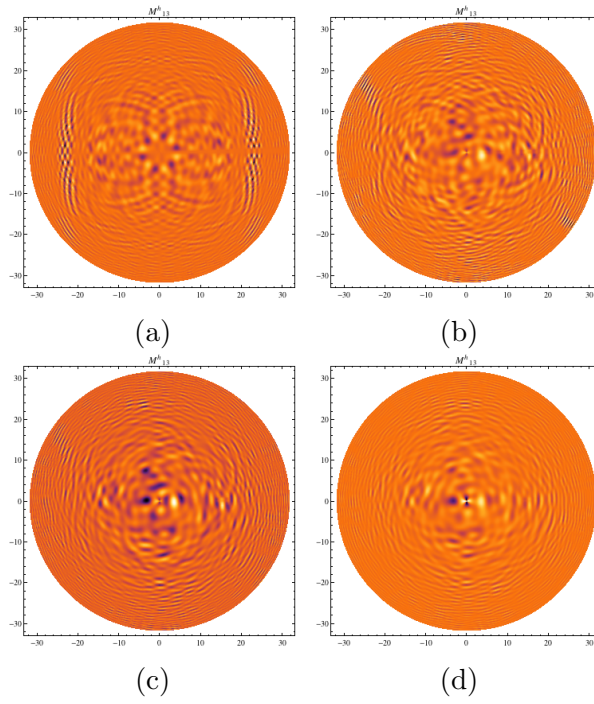
Figure 3.8: Angular distribution of M_{13}^h size parameter and Δ_r varies as in Fig 3.5
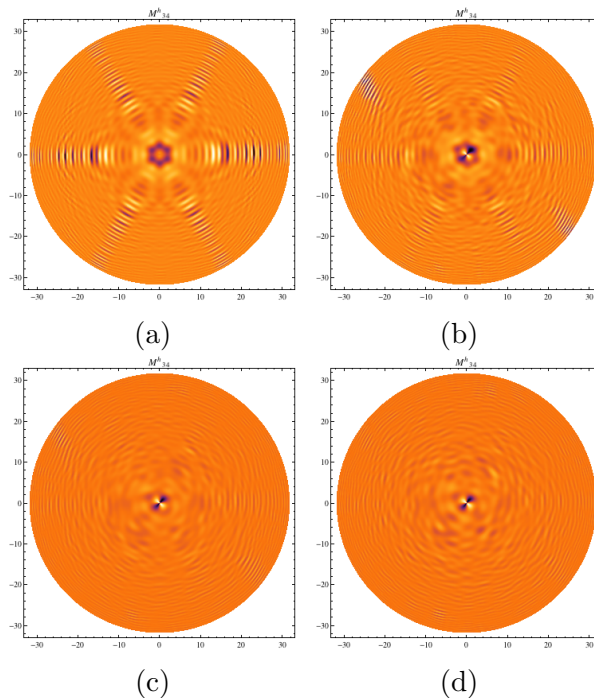
Figure 3.9: Angular distribution of M_{34}^h size parameter and Δ_r varies as in Fig 3.5

3.3   Light Scattering By Inhomogeneous Ice Crystal.

Ice particles in cirrus clouds often do not occurring pure form, but have inhomogeneities that can develop in their growth. Two principle sources of inhomogeneity are the inclusion of soot particles and the inclusion of air bubbles. A Inhomogeneous Hexagonal Mono-crystal model cooperating the Monte-Carlo ray-tracing and Mie scattering was proposed to compute the scattering of light by an ensemble of randomly oriented hexagonal ice crystals with impurities of soot and air bubbles. The single-scattering properties of inhomogeneous ice crystals with spherical or spheroidal air bubbles trapped in ice crystals are investigated by Xie etl[13] using a geometrical optics method. In the work of them, geometric optics models were used to simulate the hexagonal crystal with bubbles[12].
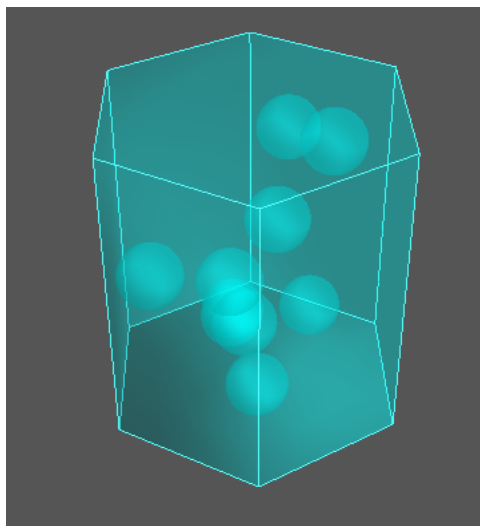
Figure 3.10: Hexagonal Prism with Bubbles

For simplicity we focus here on the inclusion of air bubbles, but our method could easily be extended to include inclusion of soot particles. The comparison with their approach will be consider in our further work. We investigate the inhomogeneous ice crystals model illustrated in Fig. 3.10, in which the bubbles are randomly distributed in the hexagonal ice crystals. Using this model, we computed the scattering of light by an ensemble of randomly oriented hexagonal ice crystals containing spherical air bubbles via PSTD. Compared with previous methods, PSTD is a full-wave method which simulates the light scattering in a more accurate way. A wave length of $0.86 \mu m$ was used in our simulations. The refractive index for ice at this wavelength is 1.3038 + i2.1500e-7. The size of the particles was set to be $10 \mu m$. We assume that the ice crystals do not have a prefer orientation. Then total of 15 orientations are chosen in the simulations. The radius of the air bubbles is set to be $2 \mu m$. The resolution of our simulation is 15. The simulation was set in two groups. Shown Fig 3.11, are results obtained for the phase matrix's dependence on volume ratioV_{ratio}:

$$V_{ratio} = \frac{V_{air}}{V_{total}} \tag{3.5}$$

Here $V_{air} = nV_{bubble}$ n is the number of bubbles, V_{bubble} is the volume for a single bubble, V_{total} is the volume of the ice crystal. V_{ratio} varies from 0% to 20%. In the other group, we analyze the the influence of bubbles' distribution on phase function, which we kept the volume ratio fixed at 20%.
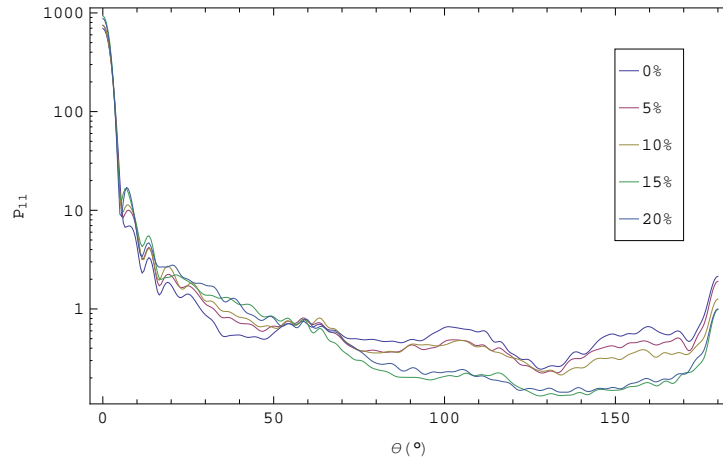

Figure 3.11: Phase function for an inhomogeneous ice crystal with various bubbles volume ratios.
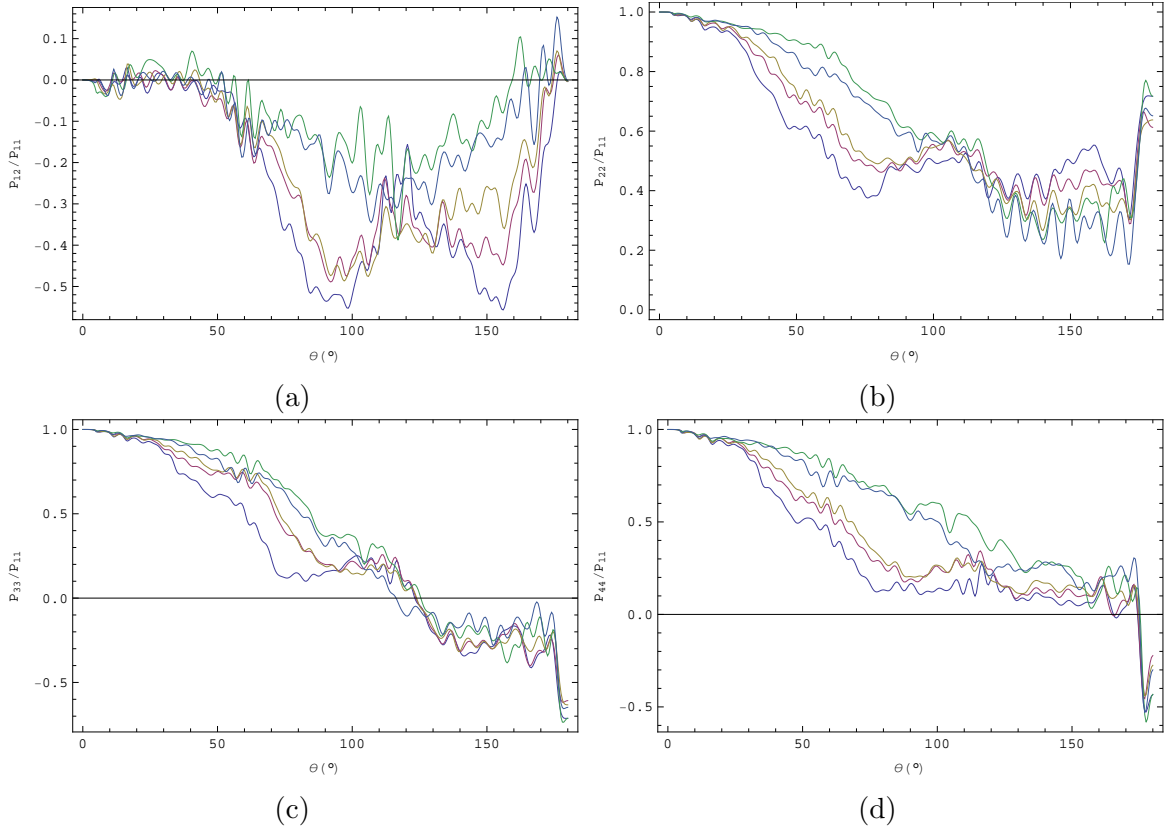
Figure 3.12: Phase matrix for inhomogeneous ice crystal with various bubble volume ratio. (Same color coding as in Fig 3.11)

Fig 3.11 shows that the phase function favors more forward scattering due to the existence of air bubbles within ice crystals, and backscattering is heavily reduced which indicates that halos may disappear if air bubbles present. As the air bubble content increases, more light are forward scattered and less are back scattered. This phenomena can be understood from a effective medium view: more bubbles dilutes effective medium, which make the ice crystal scatter softer, photons tend to transmit through instead of bouncing back. This is a quite interesting effect in radiation transfer, since less back scattering means less radiation is reflected, so the cooling effect of ice cloud will be reduced. However, Fig 3.13a shows phase functions for

simples with fixed volume ratio 20% can vary substantially, especially in the forward direction. This indicates that details of the actual spatial distribution of bubbles not just the total volume fraction, become important. Further work with larger samples is to get a reasonable estimate of the phase function. Fig 3.13b shows p12/p11, measuring the linear polarization property, for ice crystals having the volume ratio 20%.
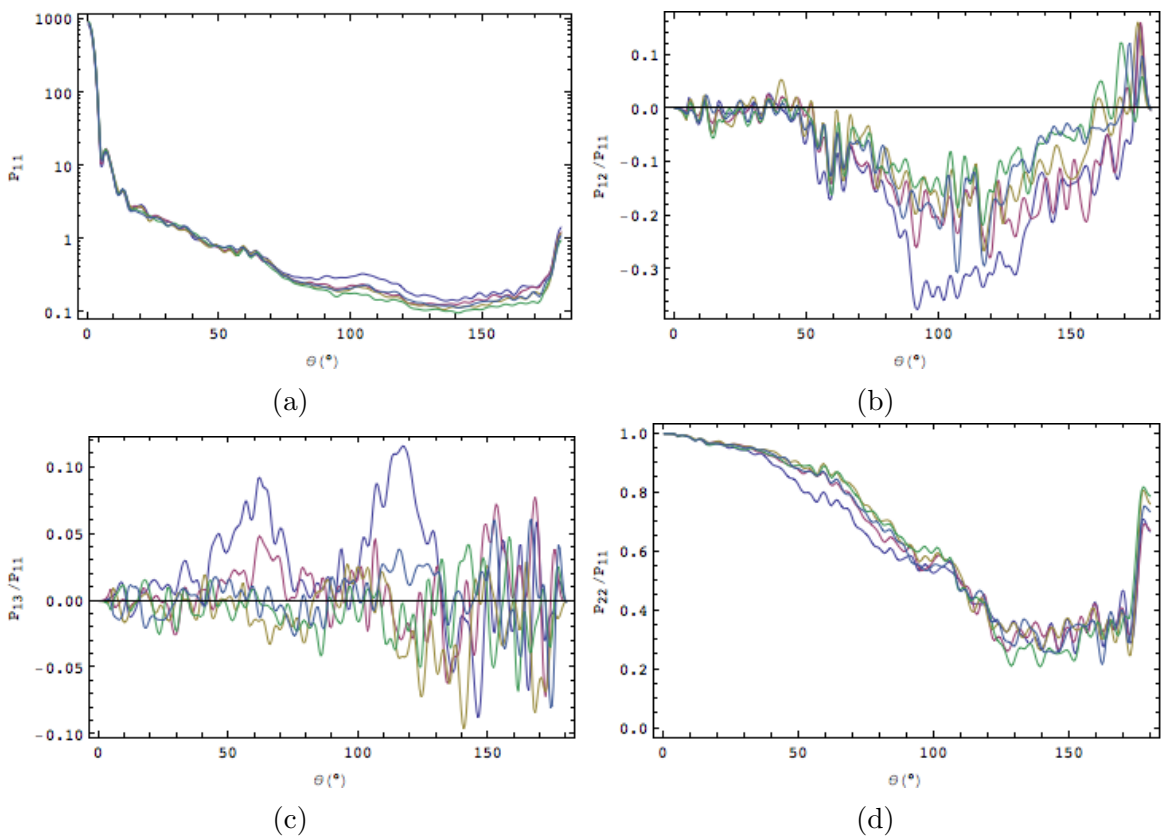

Figure 3.13: Phase matrix for inhomogeneous ice crystal with bubbles volume ratio 20%. Different color represents a different bubbles' distribution with the same volume ratio

4. SUMMARY

We have implemented a PSTD algorithm with CPML and compared its performance with the Mie's solution for simulating scattering by a dielectric sphere . The results illustrate its good performance. Further study may involve comparing the reflection error for PSTD with CPML vs UPML. More tests are still need for certification of the validity of our CPML-PSTD. We proposed a model for horizontally oriented ice crystals with roughened surfaces. Results show that the reflection ratio decreases exponentially as the roughness degree increase linearly. On the other hand, aircraft-deployed cloud imaging instruments provide a way for characterizing shapes and even surface characteristics of ice crystals. We implemented a Muller matrix holographic imaging technique for roughened particles. This imaging scheme shows potential for the cloud imaging and ice crystals investigation. The single-scattering properties of inhomogeneous ice crystals with air bubbles trapped inside have been investigated. Results showed that such inhomogeneity leads to phase function smoothing and backscattering reduction in comparison with scattering in homogeneous cases. The volume ratio was found to have a significant impact on backward scattering. As for the forward directions, some maxima are smoothed. We plan to further explore the effect of air bubble size and spatial distribution on future work.

REFERENCES

[1] G. Mie, *Beitrge zur Optik trber Medien, speziell kolloidaler Metallsungen,* Annalen der Physik **330**, 377–445 (1908).

[2] J. A. Stratton, *Electromagnetic Theory,* (McGraw-Hill, New York, 1941)

[3] M. Born and E. Wolf, *Principles of Optics,* (Cambridge, New York, 1999, 7th ed)

[4] V. D. Hulst, *Light Scattering by Small Particles,* (Dover, New York, 1981)

[5] F. M. Kahnert, *Numerical methods in electromagnetic scattering theory,* J. Quant. Spectrosc. Radiat. Transfer **79-80**, 775–824 (2003)

[6] S. Asano, *Light scattering properties of spheroidal particles,* Applied Optics **18**, 712–723 (1979).

[7] M. A. Yurkin, V. P. Maltsev, and A. G. Hoekstra, *The discrete dipole approximation for simulation of light scattering by particles much larger than the wavelength,,* J. Quant. Spectrosc. Radiat. Transfer **106** 546?557 (2007).

[8] G. Chen, P. Yang, and G. W. Kattawar, *Application of the pseudo-spectral time-domain method to the scattering of light by nonspherical particles,* J. Opt. Soc. Amer. A**44** (2008), 785–790.

[9] P. Yang and K. N. Liou, *Light scattering by hexagonal ice crystals: solutions by a ray-by-ray integration algorithm,* J. Opt. Soc. Amer. A **14**, 2278–2289 (1997).

[10] P. Yang and K. N. Liou, *Single-scattering properties of complex ice crystals in terrestrial atmosphere,* Contr. Atmos. Phys. **71**, 223–248(1998).

[11] L. Bi, P. Yang, G. W. Kattawar, and M. I. Mishchenko, *Efficient implementation of the invariant imbedding t-matrix method and the separation of variables*

method applied to large nonspherical inhomogeneous particles, J. Quant. Spectrosc. Radiat. Transfer **116**, 169–183 (2013).

[12] L. C.-Labonnote,G. Brogniez,J-C. Buriez, and M. D.Boucher *Polarized light scattering by inhomogeneoushexagonal monocrystals:Validation with ADEOS-POLDER measurements,* J. Geo. Research **106**, 12139-12153 (2001).

[13] J. D. Jackson, *Effect of the inhomogeneity of ice crystals on retrieving ice cloud optical thickness and effective particle size,* J. Geophys Res.**114** (2009), D11203.

[14] C. Zhou., P. Yang, A. E. Dessler, Y. Hu and B. A. Baum, *Study of Horizontally Oriented Ice Crystals with CALIPSO Observations and Comparison with Monte Carlo Radiative Transfer Simulations,* J. Appl. Meteorol. Climatol. **51**, 1426–1439 (2012).

[15] David A. Kopriva, *Implementing Spectral Methods for Partial Differential Equations,* (New York, Springer, 2009).

[16] S. D. Gedney *Introduction to the Finite-Difference Time-Domain (FDTD) Method for Electromagnetics,* (Morgan & Claypool, San Diego, CA, 2011).

[17] P. Yang and K. N. Liou, *Finite-difference time domain method for light scattering by small ice crystals in three-dimensional space,,* J. Opt. Soc. Amer. A **13** 2072–2085 (1996).

[18] Q. H. Liu, *The pstd algorithm: A time-domain method requiring only two cells per wavelength,* Microw. Opt. Tech. Lett. **15** (1992), 158–165.

[19] W. Sun, G. Videen, Q. Fu and Y. Hu, *Scattered-field FDTD and PSTD algorithms with CPML absorbing boundary conditions for light scattering by aerosols,* J. Quant. Spectrosc. Radiat. Transfer **131**, 166–174 (2013).

[20] J. P. Berenger, *A perfectly matched layer for the absorption of electromagnetic-waves,* J. Comput. Phys. **114**, 185–200 (1994).

[21] J. P. Berenger, *Three-dimensional perfectly matched layer for the absorption of electromagnetic waves,* J. Comput. Phys. **127** 363–379 (1996).

[22] W. C. Chew and W. H. Weedon,*A 3d Perfectly Matched Medium from Modified Maxwells Equations with Stretched Coordinates,* Microwave and Optical Technology Letters, **7** 599–604(1994).

[23] A. Oskooi, S. G. Johnson, *Distinguishing correct from incorrect PML proposals and a corrected un-split PML for anisotropic, dispersive media,* J. Comput. Phys. **230**, 2369–2377 (2011).

[24] J. A. Roden, S. D. Gedney, *Convolutional PML(CPML): An Efficient FDTD Implementation of the CFS-PML for Arbitrary Media,* Microwave and Optical Technology Letters, **27** 334–339(2000).

[25] J. Chen and J. Wang, *Convolutional Perfectly Matched Layer (CPML) for the Pseudospectral Time-Domain (PSTD) Method,* Applied Computational Electromagnetics Society Journal **28**, 680 (2013).

[26] C. Li, G. W. Kattawar, and P. Yang, *Effects of surface roughness on light scattering by small particles,* J. Quant. Spectrosc. Radiat. Transfer **89**, 123–131 (2004).

[27] Liu, C., R. L. Panetta, and P. Yang, *The effects of surface roughness on the scattering properties of hexagonal columns with sizes from the Rayleigh to the geometric optics regimes,* J. Quant. Spectrosc. Radiat. Transfer **129**, 169–185 (2013).

[28] A. A. Maradudin *Light Scattering and Nanoscale Surface Roughness,* (Springer, New York, 2007).

[29] Y-P Zhao, G. Wang, T-M Lu *Characterization of Amorphous and Crystalline Rough Surface – Principles and Applications,* (Academic Press, San Diego, CA, 2001).

[30] S. Schrder, A. Duparr, L. Coriand, A. Tnnermann, D. H. Penalver, and J. E. Harvey *Modeling of light scattering in different regimes of surface roughness,* Optics Express **19**, 9820-9835 (2011).

[31] B. A. Baum, P. Yang, Y. X. Hu, and Q. A. Feng, *The impact of ice particle roughness on the scattering phase matrix,*, J. Quant. Spectrosc. Radiat. Transfer **111**, 2534–2549 (2010)

[32] G. Chen, P. Yang, G. W. Kattawar and M. I. Mishchenko, *Scattering phase functions of horizontally oriented hexagonal ice crystals,* J. Quant. Spectrosc. Radiat. Transfer **100**, 99–102 (2006)

[33] C. Zhou., P. Yang, A. E. Dessler and F. Liang, *Statistical properties of horizontally oriented plates in optically thick clouds from satellite observations,* IEEE Geoscience and Remote Sensing Lett.**10**, 986-990 (2013).

[34] B. J. Thompson, *Holographic particle sizing techniques,* J. Phys. E **7**, 781–788 (1974).

[35] M. Gao, P. Yang, D. McKee, and G. W. Kattawar , *Mueller matrix holographic method for small particle characterization: theory and numerical studies,* Applied Optics **52**, 5289–5296 (2013).

[36] W. C. Pfalzgraff, R. M. Hulscher, and S. P. Neshyba, *Scanning electron microscopy and molecular dynamics of surfaces of growing and ablating hexagonal ice crystals,* **10** 2927–2935 (2010).

[37] A. Lang, J. Potthoff, *Fast simulation of Gaussian random fields,* arXiv:1105.2737 (2011).

[38] A. Zee *Quantum Field Theory in a Nutshell,* (Princeton, NJ, 2010), 2nd ed.

[39] L. Tsang and A. Ishimaru *Backscattering enhancement of random discrete scatterers,* J. Opt. Soc. Amer. A **1**, 836-839 (1984).

[40] T.H. Beuman, A.M. Turner, and V. Vitelli, *Stochastic geometry and topology of non-Gaussian fields,* Proc. Natl. Acad. Sci. **109** (2012), 19943–19948.